Journal of Engineering Physics and Thermophysics, Vol. 72, No. 6, 1999

RADIATION OF STRONG SHOCK WAVES PROPAGATING IN THE EARTH'S ATMOSPHERE

K. L. Stepanov, Yu. A. Stankevich, and L. K. Stanchits

UDC 533.7:519.958

Radiation of a strong shock wave propagating in air at heights $H \leq 50$ km with velocity $D = 20-50$ km/sec is investigated. From the solution of a self-consistent radiation-gasdynamic problem with real thermodynamic and optical properties of air the distributions of gasdynamic parameters and radiant fluxes in the heating region ahead of the front and in the relaxation zone behind a viscous shock are obtained. The characteristics of radiation generated by the shock wave and going to "infinity" are determined. Calculations of integral and spectral radiation fluxes on the earth's surface at different stages of the motion of a large asteroid in the atmosphere are given.

Meteoric bodies move in the Earth's atmosphere with velocities in the range $V \sim 10-70$ km/sec. In the upper layers of the atmosphere the interaction with the ambient medium occyrs in the regime of free molecular flux; as the height decreases, we observe a transition to a gasdynamic regime accompanied by the formation of a strong shock wave (SW) (according to [1], for bodies with a diameter of $\gtrsim 10$ m the regime changes at heights of 120–100 km). Behind the shock-wave front (SWF), the air is heated to the temperature $T \sim 10^4-10^5$ K, is strongly ionized, and becomes the source of intense radiation with characteristic flux densities $S \sim 10^9$ W/cm^2. The basic processes that govern the structure of a shock wave of such intensity are dissociation and ionization of the gas, elastic collisions of electrons with heavy particles ensuring relaxation of the temperatures of electronic and ionic subsystems to a unified plasma temperature, electron heat conduction, and radiation transfer. The transfer of radiant energy has an effect on the dynamic parameters of flow and its space scales and governs the ablation of the meteoric body surface. The vapor produces the inhomogeneity of the plasma as far as the chemical composition is concerned and can change the intensity of SW radiation.

The problem of the structure of a plane radiating SW is among the classical problems of radiation gasdynamics. We note here the seminal works by Zel'dovich [2] and Raizer [3, 4], in which consideration was given to the qualitative pattern of gas flow in the front of a strong radiating SW and the existence of density and temperature discontinuities was proved. In [5], calculations of the structure of an SW in air of normal density were performed, in which the spectral properties of radiation were described using 38 groups while the angular radiation distribution was prescribed approximately (according to the cosine law). A complete classification of SWs in radiating gas is given in [6]. Nonstationary radiating SWs generated by a flat piston are modeled in [7-9]. If the piston velocity is constant, the asymptotic step of the problem considered describes the SWF structure. Results of experimental investigations of the radiation properties of large-amplitude shock waves in gases are contained in [10].

In [11-14], an analysis of the set of physical and radiation-gasdynamic processes in strong radiating shock waves is made, which showed that the description of the wave structure as a first approximation reduces to the problem of radiation relaxation on the SW front. Its solution in the diffusion approximation for a "gray" gas [11-13] permits determining the distribution of gasdynamic and radiation parameters ahead of a viscous shock and in the relaxation zone behind it. The profiles calculated are employed to construct a self-consistent solution with the optical characteristics of a real spectrum [11, 14]. Given below are a brief formulation of the problem and the

Academic Scientific Complex "A. V. Luikov Heat and Mass Transfer Institute," National Academy of Sciences of Belarus, Minsk, Belarus. Translated from Inzhenerno-Fizicheskii Zhurnal, Vol. 72, No. 6, pp. 1149-1158, November–December, 1999. Original article submitted March 10, 1999; revision submitted May 12, 1999.

1062-0125/99/7206-1111$22.00

TABLE 1. Rosseland and Planck Radiation Paths behind an SWF

H, km	50	40	30	20	10
L_R, cm	10^2–10^3	10^1–$3\cdot10^2$	10^0–$3\cdot10^1$	$3\cdot10^{-2}$–10^0	10^{-2}–10^{-1}
L_P, cm	10^0–10^1	$3\cdot10^{-1}$–$3\cdot10^0$	10^{-1}–10^0	$3\cdot10^{-2}$–$3\cdot10^{-1}$	10^{-3}–10^{-2}

results of calculating the radiation of a plane SW for different heights and velocities of its motion. The radiation fluxes on the Earth's surface generated in the motion of a large asteroid in the atmosphere are evaluated.

Structure and Radiation of Strong SWs. Analysis shows [11, 12] that the largest length scale in the problem of the structure of a radiating SW is associated with the thermal-radiation paths of a plasma (the characteristic quantum energies are $E \sim (2-5)T$). The radiation mean free path exceeds the characteristic dissociation L_d and ionization L_i lengths of air [15]. It also exceeds the scale of the region of relaxation of the electron and heavy-particle temperatures to a unified plasma temperature [16] and the length of the zone where electron heat conduction is substantial [17]. When the characteristic relaxation lengths differ markedly in magnitude, analyzing the SW structure is simplified considerably [18] since the terms that correspond to the processes with scales $L_i \ll L_{max}$ turn out to be small as far as the parameter L_i/L_{max} is concerned. It what follows it is assumed that dissociation and ionization processes "watch" the temperature and density of the medium, the temperatures of the electrons and the atoms (ions) are the same, and electron heat conduction is small as compared to radiant heat transfer. The structure of a strong radiating shock wave is described by the system of steady-state equations of one-dimensional plane gasdynamics and radiation transfer. In the coordinate system related to an SWF, it has the form

$$\rho u = \rho_0 D, \quad p + \rho u^2 = p_0 + \rho_0 D^2, \quad \varepsilon + \frac{p}{\rho} + \frac{u^2}{2} + \frac{S}{\rho_0 D} = \varepsilon_0 + \frac{p_0}{\rho_0} + \frac{D^2}{2} + \frac{S_0}{\rho_0 D}; \tag{1}$$

$$\mu \frac{dI_E}{dx} = \kappa_E (I_{Eeq} - I_E), \quad S_E = \int\limits_{(4\pi)} I_E \Omega \, d\Omega, \quad S = \int\limits_0^\infty S_E dE, \tag{2}$$

where the subscript 0 refers to the equilibrium state of the gas ahead of the front; D is the velocity of the unperturbed gas relative to the SWF. The solution of Eqs. (1)-(2) that determines the spatial distribution of all the quantities and the flux S_0 going from the SWF to "infinity" depends on the parameters of the unperturbed medium (ρ_0, p_0) and the wave velocity D. Very far behind the SW, the parameters of flow correspond to the equation of a shock adiabat; the radiation flux is absent ($S_1 = 0$). Indeed, for heights $H \leq 50$ km, the characteristic temperatures behind the front are in the range $T = 2-9$ eV, and the compression ratios are $\rho/\rho_0 = 10-14$. The corresponding Rosseland and Planck mean free paths of radiation behind the SWF are given in Table 1. It shows that when $H =$ 50 km the largest Rosseland paths have order $L_R < 10^3$ cm and decrease sharply with height. The Planck mean free paths are generally smaller by one to two orders of magnitude than the Rosseland mean free paths. If it is taken into account that, for an asteroid body with a linear scale of ~1 km, the viscous shock is at a distance of ~100–200 m from its surface and its position depends weakly on the velocity of motion D, the assumption that the layer of compressed gas behind the front is optically thick is justified in a wide range of conditions.

Using the equation of state $p = p(\rho, T)$ and the law of conservation of momentum, we can construct relations dependent on one variable, which describe a change in the characteristics of the gas in the SW. The parameters in them are ρ_0, p_0, and D. Having selected the temperature as this variable and having determined $\varepsilon(T)$, $p(T)$, and $\rho(t)$, we find all the thermodynamic characteristics at a given spatial point from the temperature in it. Subsequently, from the equation of conservation of mass flux and energy we determine the gas velocity $u = \rho_0 D/\rho$ and the radiation flux

$$S = S_0 - \rho_0 D F(T),$$

$$F(T) = \varepsilon(\eta) - \varepsilon_0 - \frac{p_0}{\rho_0}(1-\eta) - \frac{D^2}{2}(1-\eta)^2, \eta = \rho_0/\rho = \eta(T). \tag{3}$$

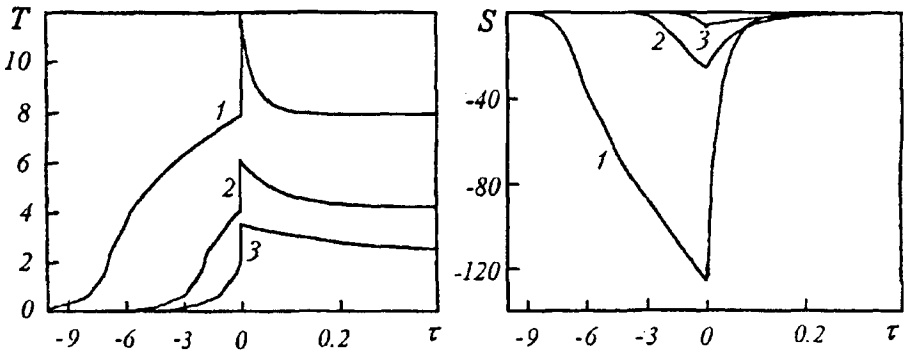

Fig. 1. Temperature and radiation-flux distributions along τ for H = 30 km and D = 50 (1), 30 (2), and 20 km/sec (3). T, eV; S, MW.

From (3) it can be seen that the spatial profile of the flux depends on S_0 in addition to ρ_0, p_0, and D. We note that the signs of the velocity D and the flux S are always opposite. The initial state ahead of the front corresponds to the flux $S = S_0$, i.e., $F(T_0) = 0$. In the equilibrium state behind the SW front, $S_1 = 0$ and $F(T_1) = S_0/(\rho_0 D)$. Since $F(T_1) < 0$, the finite temperature behind the wave front will be lower than in the absence of the escaping radiation. If the luminesced energy is disregarded and the radiant flux escaping from the SW is considered to be small as compared to the hydrodynamic flux ($S_0 << \rho_0 D^3/2$), the finite temperature will also be determined by the condition $F(T_1) = 0$.

To find a self-consistent solution of the equations of radiation gasdynamics that satisfies the boundary conditions, we must construct a convergent iteration process. For this purpose, "good" initial profiles of the gasdynamic parameters are required. Their distribution can be found by considering the transfer of radiation in a "gray"-diffusion approximation [11, 13]. The corresponding equations

$$\frac{dS}{d\tau} = c\,(U_{eq} - U)\,, \quad S = -\frac{c}{s}\frac{dU}{d\tau}\,, \quad U_{eq} = \frac{4\sigma T^4}{c} \tag{4}$$

in view of (3) reduce to one equation on the phase plane of the variables $U-T$

$$\frac{dU}{dT} = -3\left(\frac{\rho_0 D}{c}\right)^2 \frac{F'(T)\,(F(T) - S_0/(\rho_0 D))}{U_{eq}(T) - U}\,, \tag{5}$$

whose detailed analysis is given in [11]. Upon solution of the problem on the phase plane, integrating the expression

$$\frac{dT}{d\tau} = \rho_0 D F(T)\left(\frac{c}{3}\frac{dU(T)}{dT}\right)^{-1}\,, \tag{6}$$

we can obtain the temperature and radiant-flux distributions along τ – the "average" optical variable reckoned from the wave front. Figure 1 shows the profiles of the temperature and the radiation flux in the wave at a height of 30 km with velocities of 50, 30, and 20 km/sec. From the figure we notice that the regime of propagation turns out to be supercritical for D = 50 km/sec (the temperature ahead of the viscous shock is $T_- = T_1$), subcritical with D = 20 km/sec ($T_- < T_1$), and near-critical for D = 30 km/sec ($T_- \approx T_1$). We note a significant difference in the optical thicknesses of the heating layer and the relaxation region behind the viscous shock; the latter turns out to be much smaller. When $D > D_{cr}$, in view of the condition $T_- = T_1$ the radiant flux on the discontinuity S_f is determined by law of conservation of energy (3) $S_f \approx -\rho_0 D F(T_1)$ ($F(T_1)$ must be taken on the branch of the function corresponding to the states with density ρ that is similar to ρ_0). The quantity D_f is independent of the spectral characteristics of radiation in the vicinity of the shock. Nonequilibrium radiation generated in an optically thin temperature peak makes a small contribution to the flux. In subscritical-amplitude waves ($D < D_{cr}$), unidirectional fluxes near the viscous compression shock differ strongly. Nonetheless, in this case, too, the flux S_f and the temperature jump $T_\pm$ are described rather well by the "gray"-diffusion approximation (the flux from the

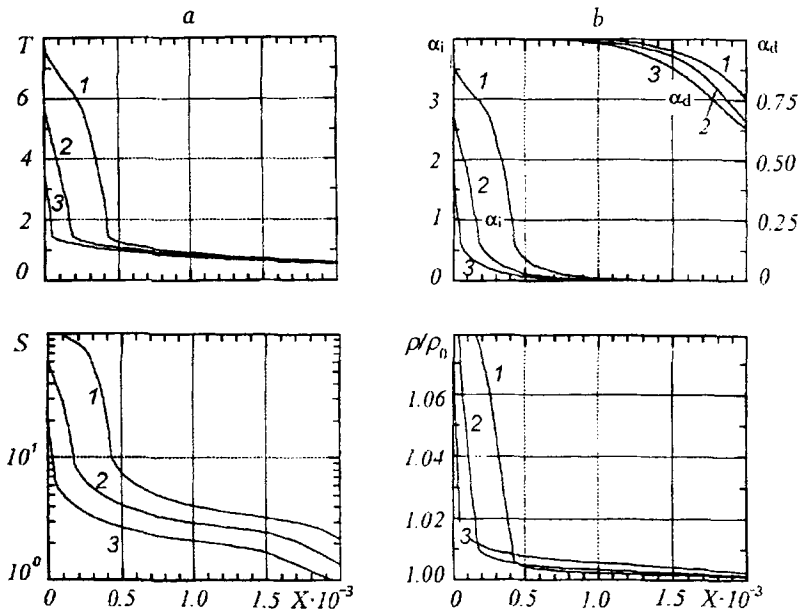

Fig. 2. Profiles of the temperature and radiation flux (a) and of the degrees of ionization α_i and dissociation α_d, and the compression ratio ρ/ρ_0 (b). H = 30 km, D = 50 (1), 40 (2), and 30 km/sec (3). X, cm.

front is similar to σT_1^4, while the flux from the heating layer to the front is small). For example, in [7], with the mass velocity of the gas behind the SWF V = 30 km/sec and the initial density of the air $\rho_0 = 1.23 \cdot 10^{-4}$ g/cm^3 (these parameters correspond to H = 18 km and D = 33 km/sec), the maximum temperature in the heating layer is T_- = 4 eV, the peak temperature is T_+ = 7.3 eV, and the flux on the front is S_f = 165 MW/cm^2. Calculations in the "gray"-diffusion approximation yield T_- = 4 eV, T_+ = 7.24 eV, and S_f = 152 MW/cm^2. The difference in the flux S_f is most probably associated with slight differences in the equation of state since, in [7], the equilibrium temperature is T_1 = 5.7 eV and, in our case – 5.56 eV.

The profiles of the gasdynamic quantities were converted from the average optical variable τ to the space coordinate x with allowance for the character of radiation transfer in various layers [11, 14]. In the waves of supercritical amplitude in the heating zone the temperature $T(\tau)$ changes weakly on the scale $\Delta\tau = 1$. The radiant heat transfer here occurs in the regime of radiant heat conduction. Therefore it is natural to use the Rosseland mean free path of radiation. The Planck mean absorption coefficient served as the conversion scale near the SWF and in the forepart of the heating zone where the radiation is strongly nonequilibrium. In the iteration process, which coordinates the energy and radiative transfer equations, it is most difficult to obtain the self-consistent solution in the vicinity of the front and at the periphery of the heating zone. Here, we have to find the absorption coefficient K that determines the relationship between the space and optical variables ($\Delta x = \Delta\tau/K$) by averaging the spectral absorption coefficient κ_ε over the self-radiation field. In calculating waves of subcritical amplitude, convergence of the solution is promoted by the weaker effect of the heating layer on the parameters of flow behind the viscous shock.

To describe radiation transfer in a real spectrum, use was made of the integral equation for a flux that is equal to the difference of unidirectional fluxes:

$$S_E^+(\tau_E) = 2\int_{\tau_0}^{\tau_E} S_{E\text{eq}}(\tau')\,[\exp(\tau' - \tau_E) - (\tau_E - \tau')\,E_1(\tau_E - \tau')]\,d\tau' + S_{E0}^+(\tau_E), \tag{7}$$

$$S_E^-(\tau_E) = 2\int_{\tau_E}^{\tau_1} S_{E\text{eq}}(\tau')\,[\exp(\tau_E - \tau') - (\tau' - \tau_E)\,E_1(\tau' - \tau_E)]\,d\tau' + S_{E0}^-(\tau_E). \tag{8}$$

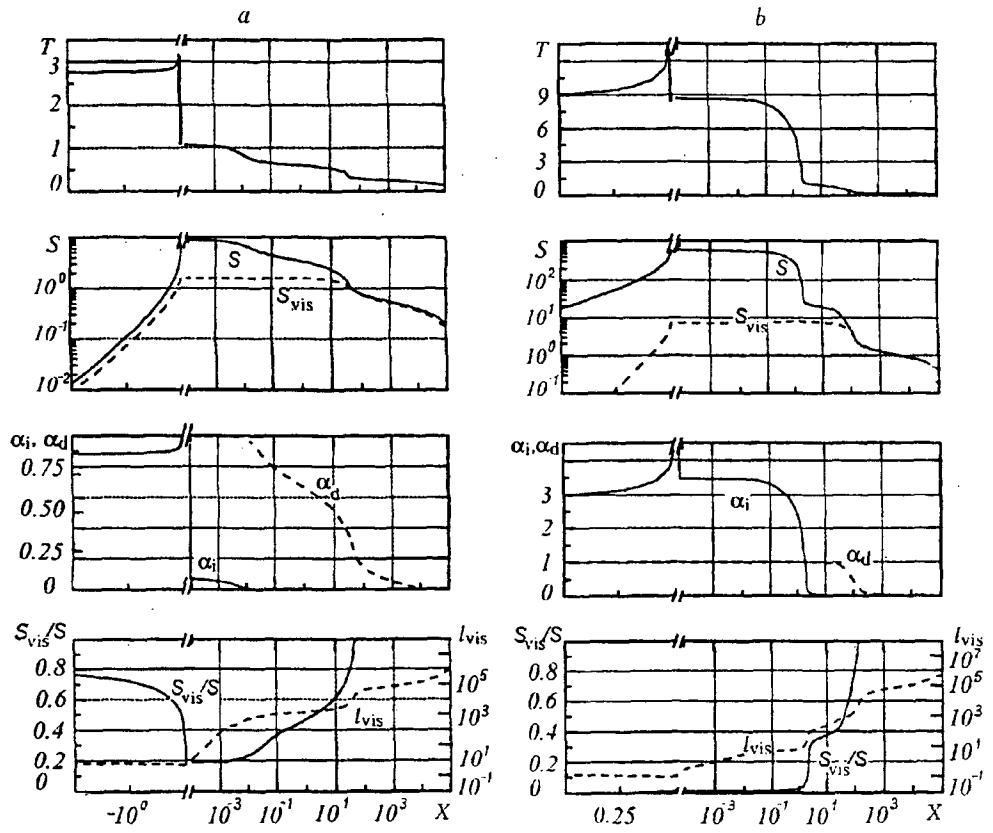

Fig. 3. Structure of an SW at the height H = 20 km for D = 20 (a) and 50 km/sec (b). l_{vis}, cm.

In numerical integration of the radiative transfer equations in the form of (7) and (8), the source function $S_{Eeq}(\tau')$ is approximated linearly inside the counting cell, which ensures reaching the limit of radiant heat conduction. We note that representation of the solution of the transfer equation in the form of a flux leads to a complex structure of expressions (7) and (8) that is manifested in the absence of a local relation between the fluxes at neighboring points. The total radiation is found by direct integration over the spectrum; 1300 spectral groups describe the range of quantum energies, in which plasma emission is substantial.

Let us consider further the results of calculations. Figure 2 (the wave is moving from left to right) presents the physical characteristics in the heating zone ahead of the shock wave at a height of 30 km. Here, for SW velocities D = 50, 40, and 30 km/sec, the distributions of the temperature, the radiant flux, the degrees of dissociation α_d and ionization α_i of air, and the compression ρ/ρ_0 ahead of the SWF are shown. Waves with these D at heights H > 30 km/sec are supercritical. Comparison of the dependences of the radiant flux and the parameters α_d and α_i shows that the maximum divergences of the flux correspond to the segments where intense dissociation and ionization of the gas occur. As is evident from the plots, in all the cases the dissociation and ionization waves are separated in space rather strongly.

Figure 3 shows the structure of shock waves with velocities of 20 and 50 km/sec at a height of 20 km. Unlike in the previous data, here the profiles of the parameters are given on both sides of the viscous shock. The gas temperature, the radiant flux S, and the radiation flux in the "visible" region of the spectrum S_{vis} (1.5 < E < 6.5 eV, to the Schumann–Runge absorption band), the degrees of dissociation and ionization of the gas, and the radiation mean free path in the "visible" range averaged over the local radiation spectrum l_{vis} are presented. The space coordinate ahead of the SW front is prescribed in a logarithmic scale and behind the front – in a linear scale. As is evident from the plot, for D = 20 km/sec the radiation of the visible range on the SWF amounts to about 15% of the total flux; at a distance of 40 cm ahead of the front the entire radiation of the SW is in the visible spectrum; the slight difference in the fluxes S and S_{vis} at large distances is associated with the fact that the total flux involves the IR spectral region. Behind the front the fraction of S_{vis} in the total flux increases,

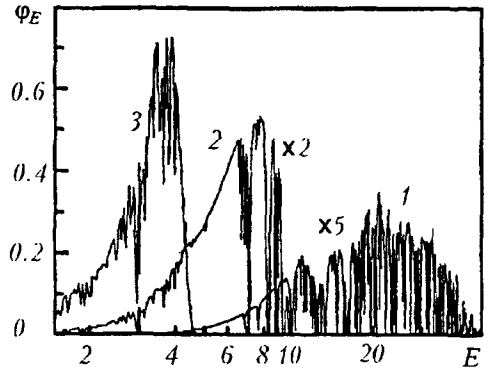

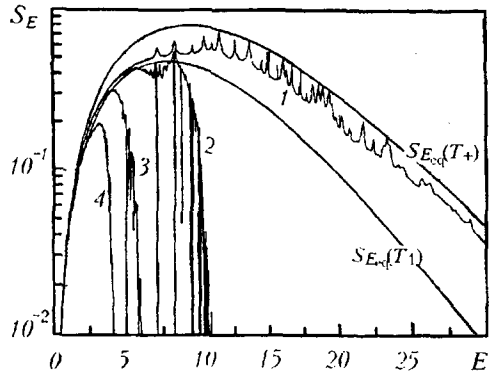

Fig. 4. Normalized function of the radiation flux of an SW (D = 50 km/sec, H = 30 km): 1) distance from the front X = 50 cm, S = 107 MW/cm^2; 2) $X = 10^3$, S = 4; 3) $X = 10^4$, S = 0.27. φ_E, eV^{-1}; E, eV.

Fig. 5. Spectral flux of SW radiation (D = 20 km/sec, H = 20 km): 1) X = 0, S = 8.76 MW/cm^2; 2) 4 cm and 2.9; 3) 55 and 0.93; 4) $9.2 \cdot 10^3$ and 0.405.

which is due to the transparency of the relaxation zone sufficient for this radiation ($l_{vis} \sim \Delta x \sim 1$ cm). Shorter-wave thermal radiation that corresponds to $T_1 \approx 2.77$ eV has smaller paths and is thermalized more rapidly. With a wave velocity of 50 km/sec the radiation S_{vis} amounts to somewhat more than 1% of the total flux from the front, and the transition to the visible range of SW radiation occurs at a distance of 10^2 cm from the front; behind the SWF the contribution of S_{vis} is slight since the scale of the relaxation zone clearly exceeds its mean free path.

The radiation spectra of shock waves at various distances from a viscous shock are presented in Figs. 4 and 5 for several parameters D and H. For the spectral functions of radiation ($\int_0^\infty \varphi_E dE = 1$) at various distances from the SWF to be comparable, φ_E (1) in Fig. 4 is increased fivefold and φ_E(2) is increased twofold. Figure 5 also shows black-body radiation corresponding to the equilibrium temperature behind the front T_1 and the peak temperature T_+. It can be seen that for quanta with $E \leq 7$ eV the temperature peak is optically transparent, and the radiation in this region is similar to Planckian radiation with T_1. The radiant flux in spectral lines is closer to $S_{Eeq}(T_+)$. On the whole, the temperature peak radiates a spectrum which is characteristic of a semitransparent layer. Comparison of the spectra (Fig. 5) and the degrees of dissociation (Fig. 3) at equal distances from the front X = 4 and 55 cm shows that the dissociation wave is maintained by radiation with a quantum energy in the range E = 6.5–11 eV.

In waves of supercritical amplitude, because of the high opacity of the region heated ahead of the front the flux that goes to "infinity" is formed in its peripheral part while the radiation of hot layers is shielded. In subcritical SWs, the flux going to "infinity" is radiated from the SW front, and the heating tongue can shield it only partially. For example, at height H = 0 the temperature ahead of the viscous shock is T_- = 5.08, 2.57, 1.13, and 0.43 eV for D = 50, 40, 30, and 20 km/sec, respectively; the air ahead of the SW is partially dissociated and ionized. Therefore shielding of the radiation going from the wave front is substantial in the heating zone. Here it is converted to thermal radiation with lower T.

When the radiation going to "infinity" is analyzed, the absorption coefficient as a function of the quantum energy at low temperatures is of fundamental importance. As is known [19-21], absorption increases sharply behind the ionization thresholds of the fundamental components of air; this causes the radiation to shift to a softer region of the spectrum with distance from the front (Figs. 4 and 5). At rather far distances, the entire radiation is concentrated in the visible region. The absorption coefficient in it is small as compared to the remaining segments of the spectrum where the SW radiates. At temperatures of $\sim 10^3$ K the absorption coefficient remains practically constant with T [22] while its dependence on the quantum energy E and the density can be approximated by the expression

TABLE 2. Fluxes in SW: $S_g = \rho_0 D^3/2$, S_0 (MW/cm^2), and $\alpha = S_0/S_g$ (%)

H, km		D, km/sec				
		50	40	30	20	10
50	S_g	6.375	3.264	1.377	4.08–1	5.1–2
	S_0	1.2–2	9.7–3	7.2–3	4.8–3	2.5–3
	α	1.88–1	2.97–1	5.23–1	1.18	4.9
40	S_g	2.54+1	1.30+1	5.495	1.628	2.035–1
	S_0	5.2–2	4.1–2	3.1–2	2.07–2	1.04–2
	α	2.05–1	3.4–1	6.16–1	1.39	5.1
30	S_g	1.15+2	5.888+1	2.484+1	7.360	9.20–1
	S_0	2.55–1	2.03–1	1.53–1	1.02–1	4.7–2
	α	2.22–1	3.45–1	6.2–1	1.4	5.1
20	S_g	5.556+2	2.845+2	1.200+2	3.556+1	4.445
	S_0	1.32	1.08	8.08–1	5.37–1	1.0–1
	α	2.37–1	3.8–1	6.73–1	1.51	2.81
10	S_g	2.619+3	1.341+3	5.657+2	1.676+2	2.095+1
	S_0	6.96	5.57	4.19	2.8	1.45–1
	α	2.66–1	4.15–1	7.4–1	1.67	6.9–1
0	S_g	7.688+3	3.936+3	1.660+3	4.920+2	6.15+1
	S_0	2.21+1	17.7	12.9	8.61	1.65–1
	α	2.88–1	4.5–1	7.77–1	1.75	2.68–1

$$\log \kappa_E \,(\mathrm{cm}^{-1}) = E\,(4.33 - 0.66E) - 11.41 + 1.5 \log (\rho/\rho_0)$$

(E in eV and $\rho_0 = 1.23 \cdot 10^{-3}$ g/cm^3). The characteristic paths of radiation with $E = 3$ eV in "cold" air at heights of 50, 40, and 30 km are equal to $\sim 10^9$, 10^8, and 10^7 cm, respectively. One usually assumes that cold air is transparent to a visible light. Distinct absorption begins in the Schumann–Runge band at wavelengths $\lambda \leq 90$ mm. Large, even if finite, paths of the radiation of the visible range cause heating of the gas to temperatures $T \sim (1-3) \cdot 10^3$ K at large distances, the radiation flux decreasing exponentially. Therefore, as the heating-zone width we can take the largest physical scale, which is the distance from the SW front to the boundary of the dissociation region of the air. The radiation escaping from this boundary (conventionally $\alpha_d \approx 0.05$) is in the visible range of the spectrum; it perturbs slightly the initial parameters of the medium, and we can consider it as going to "infinity." In the absence of distinct dissociation of air in the heating layer, the radiation escaping from the SW front is virtually not shielded. In this case, the shock wave radiates as a black body with equilibrium temperature T_1, and the radiation flux at "infinity" is equal to the fraction of the visible spectrum in the total flux σT_1^4. The flux of the radiation going to "infinity" S_0 calculated in this manner and its ratio to the hydrodynamic energy flux S_g ($\alpha = S_0/S_g$) are given in Table 2. We note that in relatively weak shock waves ($D = 10$ km/sec, $H = 20$, 10, and 0 km) the gas ahead of the front is not dissociated; the radiation flux leaving the SWF is evaluated by the number $S_0 = \beta_{vis} \sigma T_1^4$.

The character of shielding the radiation of the optical range ($\lambda = 380-680$ nm) escaping from the front SW as its velocity increases is presented in Fig. 6. Here the dependences of the flux in this spectral interval obtained by calculation of the SW structure and found by the formula $S_{\Delta\lambda} = \beta_{\Delta\lambda} \sigma T_1^4$ are shown for $H = 0$, 20, and 50 km. Comparison of these data shows that the maximum of the radiation of the optical range is attained with velocities (temperatures) that are smaller than the critical values for this height. For example, with $H = 0$, $D_{cr} = 88.1$ km/sec [23] and $D_{max} = 50$; with $H = 20$ km, $D_{cr} \approx 60$ km/sec and $D_{max} \approx 39$; and with $H = 50$ km, $D_{cr} \approx 15$ km/sec while $D_{max} \approx 10$ km/sec.

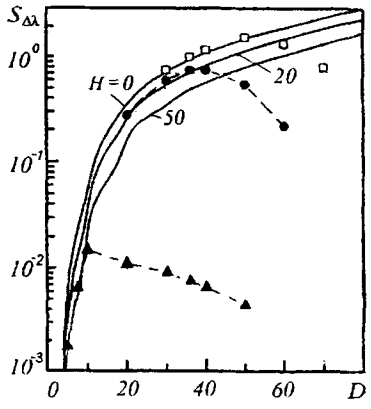

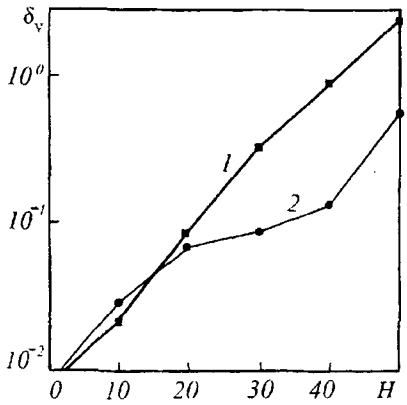

Fig. 6. Optical-radiation flux from the SW front vs. velocity. Solid curves correspond to $S_{\Delta\lambda} = \beta_{\Delta\lambda}\sigma T_1^4$, dashed curves with dark symbols correspond to numerical calculation, light symbols are the data of [15]. $S_{\Delta\lambda}$, MW/cm^2; D, km/sec.

Fig. 7. Dimensionless evaporation rate $\delta_v = Q_v/\rho_0 D$: 1) D = 50 km/sec; 2) 10. H, km.

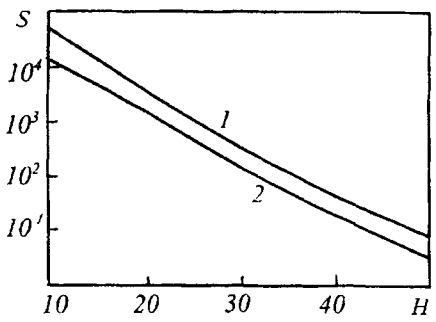

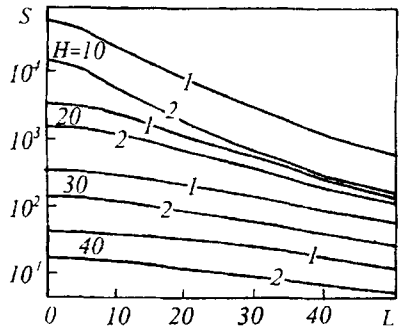

Fig. 8. Radiation flux at the epicenter vs. height of a moving body: 1) D = 50 km/sec; 20) 20. S, kW/m^2, H, km.

Fig. 9. Radiation flux on the earth's surface vs. distance L from the epicenter: 1) D = 50 km/sec; 2) 20. L, km.

Parameters of Radiation on the Earth's Surface. Radiation transfer of the energy from shock-compressed gas layers to a body governs the ablation of its surface. Analysis of the ablation processes based on the solution of the plane Stefan problem [24] permits comparison of the arrival rate of the vapor of asteroid material Q_v with the rate of arrival of air at the shock front. Figure 7 gives the dimensionless evaporation rate δ_v as a function of the weight for two velocities of the shock wave D = 50 and 10 km/sec. As is evident from the figure, for $H \leq 40$ km, $\delta_v < 1$. The internal energy of the vapor is close to the evaporation energy ($\varepsilon_v \approx 6.3$ kJ/g for Fe and $\varepsilon_v \approx 9$ kJ/g for SiO_2). With the corresponding temperatures they turn out to be rather transparent to the longwave radiation of the shock wave (more rigid radiation from the front is reabsorbed by the air layers). Accordingly, the vapor density near the surface from the condition of dynamic equilibrium (the equality of pressures) exceeds the density of the ambient air by an order of magnitude and more. Since $\delta_v < 1$ at the heights considered, the evaporated mass is retarded and is removed by the gas flux to the periphery of flow. If the accumulation of the evaporated mass at large heights is disregarded (there $\delta_v > 1$ and the vapor mass is not removed by the inflowing air flux) the evaporation pattern can be considered to be quasistationary. Then the mass of material evaporated per unit time is equal to the mass of the vapor blown off by the inflowing flux. In this case, the vapor mass is likely to be relatively small, and therefore in subsequent calculations the absorption coefficient of the vapor $\kappa_E(T, \rho)$ is assumed to be equal to its values for air.

From the one-dimensional temperature and density fields in the vicinity of the body calculated for a set of velocities D and heights H, we evaluated the radiant fluxes on the earth's surface at different stages of asteroid

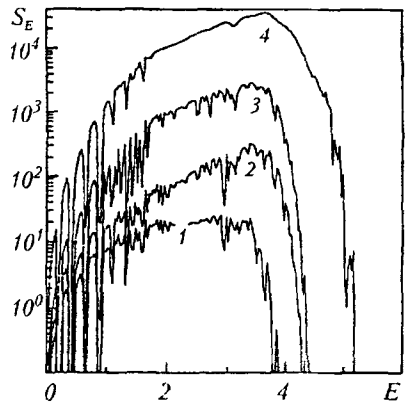

Fig. 10. Spectral radiation flux on the earth's surface at the epicenter for different heights of the motion of a body with $D = 50$ km/sec: 1) $H = 40$ km; 2) 30; 3) 20; 4) 10. S_E, kW/(m^2·eV); E, eV.

motion. Consideration was given to the case of its fall at angle $\pi/2$ to the surface. To allow for the attenuation of radiation in cold air enroute to the surface, the intensity of the radiation escaping from the heating region ahead of the shock wave was multiplied by $\exp(-\kappa_E h)$, where κ_E is the mass coefficient of absorption of the cold air at height H and $h = \int_0^H \rho(H)dH$ is the characteristic height of the atmosphere. The radiation flux at various points of the surface was determined by direct integration with respect to the quantum energy. Instead of a detailed angular integration we used the average intensity multiplied by the solid angle at which the luminous region with the characteristic diameter equal to the diameter of the body (1 km) can be seen from the point of observation. The results of this calculation are given in Figs. 8 and 9. The first figure shows the radiation flux at the point of fall (the epicenter) as a function of the height of body motion. The second figure presents the flux as a function of the distance to the epicenter for different heights of body motion. We note that the optical characteristics of the cold air were determined from the transmission of solar radiation by the atmosphere [25, 26]. The spectral parameters of radiation on the Earth's surface at the epicenter are given in Fig. 10. It can be seen that as H decreases the radiation spectrum on the surface becomes more rigid. This is due both to the temperature increase behind the shock-wave front with decreasing height and the decrease in the shielding action of the earth's atmosphere.

The work was carried out under the program of the International Science and Technology Center, project B23-96.

NOTATION

D, shock-wave velocity; ρ, density; p, pressure; ε, specific internal energy; T, temperature; u, gas velocity relative to the shock-wave front; S, radiation-energy flux; I_E, spectral intensity of radiation; $I_{E\text{eq}}$, equilibrium intensity; S_f, radiant flux on the viscous shock; η, reciprocal of compression; τ, optical thickness; U, density of radiation energy; U_{eq}, density of equilibrium-radiation energy; c, velocity of light; κ_E, spectral absorption coefficient; Ω, direction of photon propagation; μ, cosine of the angle between the direction of photon propagation and the normal to the SWF; $S_{E\text{eq}}$, density of the equilibrium-radiation flux; α_d and α_i, degrees of dissociation and ionization; E, quantum energy; λ, wavelength; $T_{\pm}$, temperatures behind and ahead of the viscous compression shock; L_i, space scale of ionization; L_d, dissociation length; L_R, Rosseland mean free path of radiation; L_p, Planck mean free path; β_{vis}, fraction of radiation of the visible range in the black-body radiation flux; S_{vis}, flux of radiation of the visible spectrum; l_{vis}, mean free path of radiation of the visible spectrum; S_g, hydrodynamic energy flux in an SW; S_0, radiation-energy flux going to "infinity"; σ, Stefan–Boltzmann constant. Subscripts: 0 corresponds to the states of equilibrium ahead of the SW and 1 – behind it; $E_1(x)$, integral exponential function; δ_v, dimensionless evaporation rate.

REFERENCES

1. V. A. Bronshtén, *Physics of Meteoric Phenomena* [in Russian], Moscow (1981).
2. Ya. B. Zel'dovich, *Zh. Éksp. Teor. Fiz.*, **32**, Issue 5, 1126-1135 (1957).
3. Yu. P. Raizer, *Zh. Éksp. Teor. Fiz.*, **32**, Issue 6, 1528-1535 (1957).
4. Yu. P. Raizer, *Zh. Éksp. Teor. Fiz.*, **33**, Issue 1, 101-109 (1957).
5. J. Zinn and R. C. Anderson, *Phys. Fluids*, **16**, No. 10, 1639-1644 (1973).
6. V. V. Aleksandrov and V. P. Koterov, *Zh. Vych. Mat. Mat. Fiz.*, **12**, No. 3, 700-713 (1973).
7. I. V. Nemchinov, V. V. Svetsov, and V. V. Shuvalov, *Prikl. Mekh. Tekh. Fiz.*, No. 5, 86-92 (1978).
8. I. V. Nemchinov, V. V. Svetsov, and V. V. Shuvalov, *Zh. Prikl. Spektrosk.*, **30**, No. 6, 1086-1092 (1979).
9. I. V. Nemchinov, V. V. Svetsov, and V. V. Shuvalov, *Zh. Vych. Mat. Mat. Fiz.*, **31**, No. 6, 901-921 (1991).
10. M. A. Tsikulin and E. G. Popov, *Radiation Properties of Shock Waves in Gases* [in Russian], Moscow (1977).
11. K. L. Stepanov, L. K. Stanchitz, and Yu. A. Stankevich, *Structure of Radiating Strong Shock Waves Propagating in the Earth's Atmosphere*, Preprint No. 2 of the Academic Scientific Complex "A. V. Luikov Heat and Mass Transfer Institute," National Academy of Sciences of Belarus [in Russian], Minsk (1998).
12. K. L. Stepanov, L. K. Stanchits, and Yu. A. Stankevich, in: *Proc. of the Conf. on Low-Temperature Plasma Physics LTPP-98*, Petrozavodsk (1998), pp. 281-285.
13. K. L. Stepanov, L. K. Stanchits, and Yu. A. Stankevich, *Publ. Observ. Astron.*, Belgrade, No. 61, 163-166 (1998).
14. K. L. Stepanov, L. K. Stanchits, and Yu. A. Stankevich, *Publ. Observ. Astron.*, Belgrade, No. 61, 167-170 (1998).
15. L. N. Panasenko, G. S. Romanov, Yu. A. Stankevich, and K. L. Stepanov, *Inzh.-Fiz Zh.*, **66**, No. 4, 569-575 (1995).
16. Yu. A. Stankevich and K. L. Stepanov, in: *Abstr. of Papers submitted to the 4th Interstate Symp. on Radiation Plasmadynamics*, Moscow (1997), pp. 31-32.
17. N. N. Magretova, N. T. Pashchenko, and Yu. P. Raizer, *Prikl. Mekh. Tekh. Fiz.*, No. 5, 11-21 (1970).
18. A. L. Velikovich and M. A. Liberman, *Physics of Shock Waves in Gases and Plasma* [in Russian], Moscow (1987).
19. G. S. Romanov, Yu. A. Stankevich, L. K. Stanchits, and K. L. Stepanov, *Int. J. Heat Mass Transfer*, **36**, No. 3, 545-556 (1995).
20. G. S. Romanov, Yu. A. Stankevich, L. K. Stanchits, and K. L. Stepanov, *Inzh.-Fiz. Zh.*, **68**, No. 2, 291-305 (1995).
21. I. V. Avilova, L. M. Biberman, V. S. Vorob'ev, et al., *Optical Properties of Hot Air* [in Russian], Moscow (1970).
22. R. K. M. Landshoff and J. L. Magee, *Thermal Radiation Phenomena*, Vol. 1. *Radiative Properties of Air*, N. Y.-W. (1969).
23. Ya. B. Zel'dovich and Yu. P. Raizer, *Physics of Shock Waves and High-Temperature Hydrodynamic Phenomena* [in Russian], Moscow (1966).
24. V. E. Okunev, G. S. Romanov, and Yu. A. Stankevich, in: *Heat and Mass Transfer 98/99* [in Russian], Minsk (1999), pp. 221-225.
25. D. Rees (ed.), *Cospar International Reference Atmosphere 1986* (1989).
26. *Atmosphere: A Handbook (Reference Data and Models)* [in Russian], Leningrad (1991).